IEEE Access
Multidisciplinary ⋮ Rapid Review ⋮ Open Access Journal

Received 25 June 2024, accepted 12 July 2024, date of publication 16 July 2024, date of current version 29 July 2024.

Digital Object Identifier 10.1109/ACCESS.2024.3429347

RESEARCH ARTICLE

ANN-Based Robust Current Controller for Single-Stage Grid-Connected PV With Embedded Improved MPPT Scheme

PRABHAT RANJAN BANA[1], SALVATORE D'ARCO[2], AND MOHAMMAD AMIN[3], (Senior Member, IEEE)

[1]Department of Electric Energy, Norwegian University of Science and Technology, 7491 Trondheim, Norway
[2]Department of Energy Systems, SINTEF Energy Research, 7034 Trondheim, Norway
[3]Enchanted Rock Management LLC, Houston, TX 77002, USA

Corresponding author: Prabhat Ranjan Bana (prabhat.r.bana@ntnu.no)

This work was supported by the Department of Electric Energy, Norwegian University of Science and Technology (NTNU), Norway.

ABSTRACT There has been growing interest in single-stage grid-connected photovoltaic (PV) systems due to their reduced losses and overall size, as they eliminate the intermediate DC-DC conversion stage. The primary objective of this research is to develop a more efficient and industry-oriented control strategy for these systems. This study proposes an artificial neural network (ANN)-based controller to address the high complexity and computational demands of traditional model predictive control (MPC) methods. The ANN-controller simplifies the process by utilizing basic linear equations, significantly reducing the computational burden. Additionally, it integrates an improved maximum power point tracking (MPPT) algorithm to ensure optimal power extraction from the PV panels while maintaining excellent transient performance. The methodology involves validating the superior control performance of the proposed ANN-based strategy in a simulation environment. This includes comparisons with a benchmark grid-tied PV system managed by three different controllers, demonstrating the robustness of the ANN-controller under realistic irradiation-temperature patterns. Results show that the ANN-controller achieves faster response and improved performance compared to traditional MPC methods. Finally, the effectiveness of the ANN-based control logic is experimentally validated using a Control Hardware-In-the-Loop (C-HIL) setup, proving its practicality and reliability in real-world applications.

INDEX TERMS Artificial neural network, maximum power point tracking, model predictive control, solar photovoltaic, supervised learning.

I. INTRODUCTION

Power electronic converters are crucial for integrating renewable energy sources into the grid [1]. The single-stage grid-tied (SSGT) solar photovoltaic (PV) system has gained popularity due to its lower installation and maintenance costs, reduced system size, and higher efficiency [2], [3]. However, designing robust control strategies for SSGT systems is more challenging than for double-stage PV systems due to varying environmental conditions and grid disturbances [4]. The PV system's $P-V$ and $I-V$ profiles are highly influenced by changes in irradiance, necessitating advanced maximum power point tracking (MPPT) algorithms to maximize power extraction. Traditional MPPT algorithms like perturb & observe (P&O) and incremental conductance (InC) are simple to implement but fail to operate at the global maximum power point (GMPP) under partial shading conditions [5]. Optimization-based MPPT algorithms can address this issue but come with increased control complexity and longer tracking times [6], [7].

Moreover, traditional methods of controlling PV-fed voltage source converters (VSCs) face several challenges,

The associate editor coordinating the review of this manuscript and approving it for publication was Mou Chen.

© 2024 The Authors. This work is licensed under a Creative Commons Attribution-NonCommercial-NoDerivatives 4.0 License.
For more information, see https://creativecommons.org/licenses/by-nc-nd/4.0/

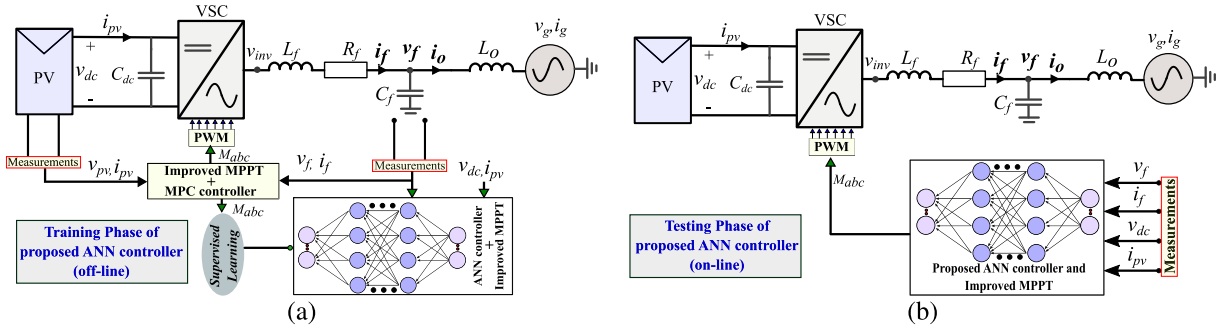

FIGURE 1. Overall block diagram of SSGT PV system with proposed ANN controller, (a) Training phase of the ANN that incorporates the MPC scheme predicting the VSC output voltage and data collection under full-state observation, (b) Testing phase of the ANN where the fully trained ANN controller is used to control the VSC by replacing the MPC scheme.

including difficulty in tuning controller gains, limited bandwidth, slow response, and stability issues [8], [9], [10]. Among various advanced control approaches, Model Predictive Control (MPC) stands out as a promising solution. MPC's key feature is its use of a system model to predict the future behavior of control variables over a specified time horizon. It then selects the optimal control action by minimizing a predefined cost function that represents the system's desired behavior [11], [12]. Despite its advantages, MPC application is hindered by the need for accurate system modeling and increased computational complexity. Additionally, determining the appropriate weight factor for the cost function often relies on trial-and-error or optimization algorithms like genetic algorithms (GA) and particle swarm optimization (PSO), which add further complexity without addressing the fundamental issue of high computational demands [13]. Efforts are ongoing to resolve these challenges by using single-step or longer prediction horizons to achieve practical and robust control performance [14].

The application of artificial intelligence (AI) to power electronics systems has garnered substantial attention in recent years due to its ability to address critical issues with inherent decision-making capabilities [15]. Neural networks (NNs) used in these systems can be classified based on their training methods into offline and online trained structures [16]. Offline training involves using simulation or experimental data sets, while online training is more suitable for complex systems where training data sets are unavailable. Among the most prominent AI and NN schemes are deep learning neural networks (DNN), reinforcement learning neural networks (RNN), deep reinforcement learning (DRL), long short-term memory RNN (LSTM-RNN), and various machine learning (ML) methods. These approaches offer excellent solutions for complex systems with diverse objectives such as energy trading, energy management in networked microgrids, inertia emulation, communication systems in microgrids, and PV forecasting [16], [17]. A comprehensive discussion on the industrial applications of ANN, considering different design and training processes, is presented in the literature [18].

For power electronics converter control, feed-forward artificial neural networks (ANN) and their variant, the multi-layer perceptron (MLP) ANN, are commonly used. For instance, ANNs have been utilized as capacitor voltage reference estimators for modular multilevel converters in three-phase systems [13], [19]. Additionally, ANNs have been adopted to simplify the multi-step prediction evaluation for model predictive control (MPC) controllers, particularly in lower-order power converter topologies [20]. Most applications of ANN in PV-interfaced power electronic generation systems are limited to maximum power point tracking (MPPT) controllers [21], [22]. ANNs have been used to replace standard MPPT algorithms for maximum power extraction and to enhance the accuracy and tracking time of global maximum power point (GMPP) without the need for additional temperature sensors [23]. However, there is limited literature on using ANN as a current controller for PV applications. One example is the use of ANN to replace the PI controller for single-phase multilevel inverter-based PV systems [24]. Another example is an ANN-based control solution for single-phase and double-stage residential PV applications, which outperforms standard vector control methods in various aspects [25].

In line with the aforementioned discussion, this paper presents an artificial neural network (ANN)-based controller for the single-stage PV system. The main contribution of the paper to the state-of-the-art comprises the following:

- An ANN-based inner-loop current controller is proposed for the single-stage grid-connected solar PV system. The ANN is trained based on the Levenberg Marquardt Back Propagation (LMBP) algorithm utilizing the MPC scheme data.
- An improved MPPT algorithm with an additional control loop is embedded with the proposed ANN controller to extract the maximum power from the PV panel for different scenarios of solar irradiance.
- Small-signal state-space model is developed to investigate the stability of the proposed ANN controller under different operating scenarios and accounting for the parameter uncertainty.

The proposed ANN controller does not involve the necessity of detailed system modelling as well as excludes solving the optimization problem or cost functions rigorously at each sampling instant. This approach has often been termed an end-to-end approach. The proposed control approach ensures

a satisfactory steady-state and faster dynamic performance than the standard PI-controller with a lesser computational burden as compared to the MPC scheme.

II. ANALYTICAL MODELING OF THE VSC WITH MPC SCHEME AND ASSOCIATED CHALLENGES

The SSGT system with ANN-based controller is trained under the supervision of MPC scheme is presented in Fig. 1. The MPC technique requires the accurate modeling of the VSC and output filter to achieve the desired performance. This section presents the modeling of the converter and a description of the equations governing the MPC scheme.

A. DISCRETE STATE-SPACE MODELING

The three-phase output voltage and current equations of the converter are modeled in the stationary $\alpha\beta$-reference frame. In this regard, each three-phase variables x_a, x_b and x_c are transformed into the corresponding $\alpha\beta$-frame by applying an amplitude invariant Clarke transformation as

$$\boldsymbol{X} = \begin{bmatrix} x_\alpha \\ x_\beta \end{bmatrix} = \mathbf{T_{abc-\alpha\beta}}\,[x_a x_b x_c]^T \tag{1}$$

where

$$\mathbf{T_{abc-\alpha\beta}} = \frac{1}{3}\begin{bmatrix} 2 & -1 & -1 \\ 0 & \sqrt{3} & -\sqrt{3} \end{bmatrix}$$

The dynamic equation of the inductor current, i_f can be expressed in state-space form as [26]

$$\frac{d\boldsymbol{i_{f,\alpha\beta}}}{dt} = \mathbf{A}\boldsymbol{i_{f,\alpha\beta}} + \mathbf{B}\boldsymbol{v_{inv,\alpha\beta}} + \mathbf{B_d}\boldsymbol{v_{f,\alpha\beta}} \tag{2}$$

where $\boldsymbol{v_{inv,\alpha\beta}} = \begin{bmatrix} v_{inv,\alpha} \\ v_{inv,\beta} \end{bmatrix}$ is the output voltage of the inverter, and $\boldsymbol{v_{f,\alpha\beta}}$ is the voltage across the filter capacitor. The bold font is used to represent the variables in matrix form. The voltages and currents are indicated in Fig. 1. The Expression of matrices $\mathbf{A}$, $\mathbf{B}$, and $\mathbf{B_d}$ are given below

$$\mathbf{A} = \begin{bmatrix} -\frac{R_f}{L_f} & 0 \\ 0 & -\frac{R_f}{L_f} \end{bmatrix},\ \mathbf{B} = \begin{bmatrix} \frac{1}{L_f} & 0 \\ 0 & \frac{1}{L_f} \end{bmatrix},\ \mathbf{B_d} = -\mathbf{B}$$

where R_f and L_f are filter resitance and inductance, respectively. Considering the above variables are maintained as constant during each sampling interval (T_s), the system described in (2) can be obtained in the discrete-time state equation as

$$\boldsymbol{i_{f,\alpha\beta}}(k+1) = \mathbf{G}\boldsymbol{i_{f,\alpha\beta}}(k) + \mathbf{H}\boldsymbol{v_{inv,\alpha\beta}}(k) + \mathbf{H_d}\boldsymbol{v_{f,\alpha\beta}}(k) \tag{3}$$

where $\mathbf{G} = e^{AT_s}$, $\mathbf{H} = (\boldsymbol{G} - \mathbf{I})\mathbf{A}^{-1}\mathbf{B}$, $\mathbf{H_d} = (\boldsymbol{G} - \mathbf{I})\mathbf{A}^{-1}\mathbf{B_d}$ and $\mathbf{I}$ is the identity matrix with same dimension as $\mathbf{G}$.

The reference current ($\boldsymbol{i^*_{f,\alpha\beta}}$) for the MPC controller is obtained as a function of dc power generated from the PV system at each sampling instant. Thus, $\boldsymbol{i^*_{f,\alpha\beta}}$ can be expressed as

$$\boldsymbol{i^*_{f,\alpha\beta}} = \frac{2}{3}\boldsymbol{T_{dq-\alpha\beta}} \cdot P_{set} \cdot \eta \cdot \frac{1}{V_d} \tag{4}$$

where V_d is the real-axis component of the output voltage on the rotating reference frame, η is the efficiency of the inverter, P_{set} and $\mathbf{T_{dq-\alpha\beta}}$ given in (5) are the instantaneous power from the PV system and the Park transformation matrix, respectively and θ is the position of the voltage vector v_f estimated with a standard phase-locked loop (PLL).

$$\mathbf{T_{dq-\alpha\beta}} = \begin{bmatrix} \cos(\theta) & -\sin(\theta) \\ \sin(\theta) & \cos(\theta) \end{bmatrix};\ P_{set} = v_{pv} \cdot i_{pv} \tag{5}$$

The single-step horizon cost function for regulation of ac current through the filter of the SSGT system can be expressed as

$$\boldsymbol{g_{con}} = \left(\boldsymbol{X}^* - \boldsymbol{X}(k+1)\right)^T \mathbf{W}\left(\boldsymbol{X}^* - \boldsymbol{X}(k+1)\right) \tag{6}$$

where $\boldsymbol{X}^* = \begin{bmatrix} i^*_{f\alpha}(k) \\ i^*_{f\beta}(k) \end{bmatrix}$, $\mathbf{W}$ is a 2×2 diagonal matrix and $\boldsymbol{X}(k+1) = \boldsymbol{i_{f,\alpha\beta}}(k+1)$ is the prediction of the state space at the next sample based on the value of the input variable v_{inv}.

Thereby, the desired modulation signal for the VSC can be obtained by taking the derivative of the cost function with respect to v_{inv} and equating it to zero. In this process, the final solution obtained is:

$$\begin{aligned} \boldsymbol{v}_{\text{inv}} = (\mathbf{H}^T\mathbf{W}\mathbf{H})^{-1}\Big[&\mathbf{H}^T\mathbf{W}\boldsymbol{X}^* \\ &- \mathbf{H}^T\mathbf{W}\mathbf{H_d}\boldsymbol{v}_{\text{f}}(k) - \mathbf{H}^T\mathbf{W}\mathbf{G}\boldsymbol{X}(k+1)\Big]. \end{aligned} \tag{7}$$

Finally, the modulation signal obtained from the above step can be sent into the PWM block to obtain the PWM signals, as shown in Fig. 1. The cost function formulation considered here can be extended even for long prediction horizon evaluation as described in [27].

B. CHALLENGES IN THE MPC SCHEME

The Model Predictive Control (MPC) scheme has certain shortcomings that limit its application, primarily due to the computational burden on the real-time controller. In a power converter, the number of switching states is represented by x^y, where x is the number of feasible states for each leg of the converter and y denotes the number of legs or phases, depending on the converter type. The standard MPC operation requires prediction and optimization procedures at each sampling instant. Consequently, the controller must predict x^y states during the prediction stage and evaluate corresponding costs during the optimization stage. In turn, the total computational burden ($N_{FCS-MPC}$) imposed by the finite control set (FCS)-MPC with prediction horizon length of 1, can be expressed as:

$$N_{FCS-MPC} = \left(\rho_p N_p + \rho_c N_c\right) x^y \tag{8}$$

where N_p and N_c are the number of calculations associated with the prediction and cost function, respectively. ρ_p (= 2) represents the number of signals that need to be predicted, and ρ_c (= 1) represents the number of objectives considered in the cost function. The (8) shows that the computational complexity of FCS-MPC increases exponentially with the number of levels and phases.

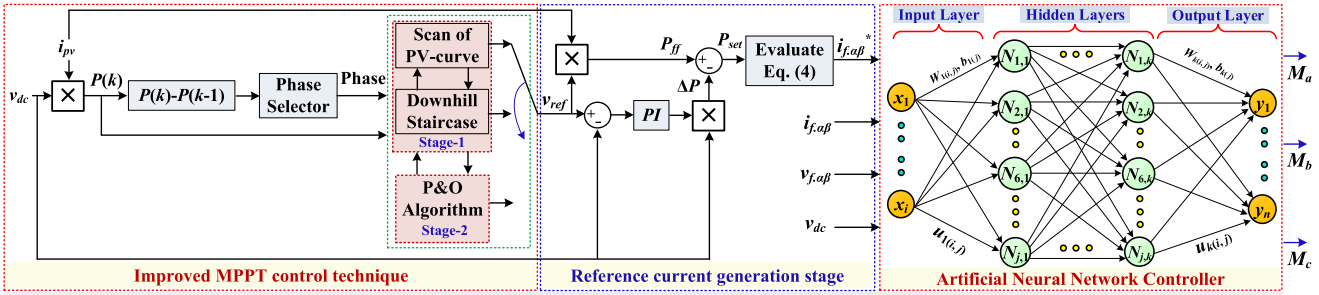

FIGURE 2. Schematic of the improved MPPT algorithm combined with the proposed ANN controller for the SSGT PV system.

Continuous control set (CCS)-MPC can provide a better control solution than FCS-MPC but with an even higher computational burden. Thus, the number of calculations ($N_{CCS-MPC}$) involved in CCS-MPC can be said to be:

$$N_{CCS-MPC} \geq N_{FCS-MPC}. \tag{9}$$

Additionally, the accuracy of the prediction function depends on precise system modeling, which further influences the optimization stage. For complex systems with multiple variables, designing an accurate higher-order mathematical model is challenging and often impractical. Therefore, an ANN controller is introduced in this work to address these issues and provide a more practical solution for MPC.

III. PROPOSED ANN CONTROLLER FOR PV SYSTEM

The off-line training phase of the ANN controller for SSGT PV system is shown in Fig. 1(a). The CCS-MPC scheme data is used for the training to retain its advantageous control features. After a successful training, the ANN controller can be deployed for the real-time testing, as illustrated in Fig. 1(b). The modeling and off-line training of the proposed ANN controller is detailed as following.

A. MODELING AND TRAINING OF ANN CONTROLLER

The ANN controller is modeled with a feed-forward supervised learning neural network structure. Training data samples of the control inputs ($i^*_{f\alpha\beta}$, $i_{f\alpha\beta}$, $v_{f\alpha\beta}$, v_{dc}) and control outputs M^*_{abc} (modulation signals) are stored in look-up table a_i and M^*_{abc}, respectively. a_i is then multiplied with the weight matrix $W_{k(i,j)}$ (i^{th} input, j^{th} node, and k^{th} layer) and added with the bias matrix $b_{k(j)}$ to procure the internal variable $u_{k(i,j)}$ as presented in (10). The output F of the hidden layer can be calculated by defining an activation function as given in (11).

$$u_{1(i,j)} = W_{1(i,j)}a_i + b_{1(j)}. \tag{10}$$

$$F\left[W_{1(i,j)}, b_{1(j)}\right] = \frac{1 - e^{-2u_{1(i,j)}}}{1 + e^{-2u_{1(i,j)}}}. \tag{11}$$

Here, $u_{k(i,j)}$ and F are termed as the control variables of the converter since they are formulated as a function of the control inputs a_i. Moreover, a linear activation function is used at the output layer, which implies the final output or predicted modulation index (M_{abc}) of the ANN is

$$M_{abc} = W_{2(i,j)}F\left[W_{1(i,j)}, b_{1(j)}\right] + b_{2(j)}. \tag{12}$$

The ANN controller is trained with the Levenberg Marquardt Back Propagation (LMBP) method by defining a cost function (c_f) as

$$c_f = \sum_{n=1}^{N}\left\{\sqrt{\left[M^*_{abc} - M_{abc}(n)\right]^2}\right\} = \sum_{n=1}^{N}\triangle M^2(n). \tag{13}$$

The goal of this training is to search for the optimum weight and bias values in order to converge at the targeted modulation signals. In this context, the gradient of the c_f with respect to weight factor and bias value is then continuously evaluated as given in (14) to find their new value.

$$\frac{dc_f}{d\vec{W}} = \sum_{n=1}^{N}\frac{d\left\{\triangle M^T(n) * \triangle M(n)\right\}}{d\vec{W}} = 2J(\vec{W})^T\triangle M \tag{14}$$

where $J(\vec{W})$ is a Jacobian matrix and can be given as

$$J(W) = \begin{bmatrix} \frac{d\triangle M(1)}{dW_1} & \cdots & \frac{d\triangle M(1)}{dW_n} \\ \vdots & \ddots & \vdots \\ \frac{d\triangle M(N)}{dW_1} & \cdots & \frac{d\triangle M(N)}{dW_n} \end{bmatrix}; \triangle M = \begin{bmatrix} \triangle M(1) \\ \vdots \\ \triangle M(N) \end{bmatrix} \tag{15}$$

Moreover, the weights of the proposed ANN controller can be updated as per (16), and similarly, the bias value can also be updated.

$$\delta\vec{W} = -\left[J(\vec{W})^T J(\vec{W}) + \mu I\right]^{-1} J(\vec{W})^T\triangle M. \tag{16}$$

$$W_{update}(W^*) = \vec{W} + \delta\vec{W}. \tag{17}$$

B. ADVANTAGE OF THE PROPOSED ANN CONTROLLER

The proposed ANN controller has several advantages like the inclusion of simple mathematical expressions, distinguished approximation, yielding generalized solution for the VSC, etc. Mainly, the ANN controller significantly reduces the complexity burden as compared to the MPC scheme.

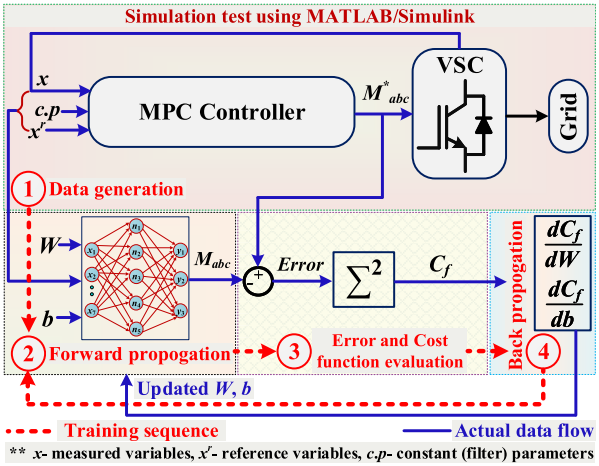

FIGURE 3. Data collection flow and offline training phase sequence of the proposed ANN controller.

The number of calculations per sampling period (N_{ANN}) associated with the ANN controller can be presented as

$$N_{ANN} = 2ij + 2jl + \lambda_1 j + \lambda_2 l \tag{18}$$

where i = number of inputs, j = number of neurons in the hidden layer, l = number of outputs, λ_1 = number of evaluation of activation function in hidden layer, and λ_2 = number of evaluation of activation function in output layer [13].

From the expressions given in (8), (9), and (18), it is evident that the number of calculations per sampling time in the MPC scheme increases at an exponential rate with the system order, whereas it is moderate in case of ANN controller.

IV. EMBEDDED IMPROVED MPPT ALGORITHM

The traditional P&O and InC MPPT algorithms do not guarantee the GMPP operation during the partial shading condition of the SSGT PV system [23]. Therefore, an improved MPPT algorithm embedded with the proposed ANN controller is presented in this work for the accurate tracking of GMPP, as illustrated in Fig. 2. The improved MPPT algorithm is a two-stage concept in which the first stage is solely dedicated to performing a full scan operation of the PV-curve. The second stage of the algorithm is the P&O method which utilizes the outcome of the first stage to locate the GMPP. The fundamental concept of the whole algorithm is detailed in the following steps.

1) In the scanning operation, the entire PV-curve is divided into different segments and the total number of segments can be calculated as

$$N_{seg} = (V_{PV}^{High} - V_{PV}^{Low})/V_{step} \tag{19}$$

where V_{PV}^{High} is the upper voltage limit beyond which there is no LMPP, V_{PV}^{Low} is the lowest possible dc voltage allowed for the converter to have a stable operation, and V_{step} (=20, in this work) is the step voltage for the uphill staircase.

TABLE 1. Eigenvalues for the SSGT-PV system.

Modes	Eigenvalues	Dominant states	Relative contribution
$\lambda_{1,2}$	$-201.5 \pm j8179.2$	v_f, i_o	0.40, 0.31
$\lambda_{3,4}$	$-222.6 \pm j7295.6$		0.40, 0.37
$\lambda_{5,6}$	$-75.7 \pm j464.3$	i_f	0.37, 0.19
$\lambda_{7,8}$	$-478.8, -500$	LPF of PLL	1, 0.96
$\lambda_{9,10}$	$-17.6 \pm j32.8$	integrator of PLL	0.47, 0.43
$\lambda_{11,12}$	$-1.8 \pm j13.0$	dc-side dynamics	0.42, 0.18

2) The operating point is then gradually shifted to the subsequent segment by recording the power value of each segment. The highest power value recorded in a segment indicates the higher chance of GMPP laying in the corresponding segment. The reference voltage of the MPP inside the vector is also extrapolated, which acts as the starting point for the P&O algorithm in the second stage. Moreover, the shifting process forces the dc voltage v_{dc} to follow the reference dc voltage v_{ref} as following

$$v_{ref} = V_{PV}^{Low} + V_{step}/N_{seg}. \tag{20}$$

3) Afterwards, v_{dc} will get close to v_{ref} with a downhill voltage step size V_{step}, which can be initialized based on the system requirement. It is worth mentioning that, selecting a relatively V_{step} possibly results in better tracking accuracy, but also in a trade-off with slower tracking speed and more dynamic power loss during the tracking process.

4) The above three steps are responsible for the first-stage scanning operation. Moreover, the first stage makes the operating point to fall in the GMPP segment. The second stage of the algorithm is enabled when v_{dc} attains the v_{ref} value. The classical P&O algorithm is then applied in the second stage to follow the MPP.

v_{ref} is obtained from the improved MPPT algorithm by following the above procedure, which is detailed in [28]. However, in this work, v_{ref} is additionally processed through an external PI-control to generate the current reference signal for the proposed ANN controller, as shown in Fig. 2. ΔP is obtained from v_{dc} multiplied to Δi obtained from the PI-control as given by

$$\Delta P = v_{dc}\left(v_{ref} - v_{dc}\right)\left(K_p + \frac{K_i}{s}\right). \tag{21}$$

ΔP is then subtracted from the feed-forward power factor P_{ff} to calculate the reference power value P_{set}, which can be written by

$$P_{set} = P_{ff} - \Delta P\,;\, P_{ff} = v_{ref}\, i_{pv}. \tag{22}$$

V. SMALL-SIGNAL ANALYSIS OF THE PROPOSED CONTROLLER

The small-signal characteristics of the proposed control has been studied to understand its interaction behavior with the SSGT PV system. It can be represented in the state-space

TABLE 2. Parameters of the SSGT PV system and proposed controller.

System Parameters	Value	Control Parameters	Value
Rated PV power P_{PV}	100 kW	Control sample time (T_{cs})	100 μs
Open circuit and MPP voltage (V_{oc}, V_{mp})	64.2, 54.7 V	Input neurons (i)	7
Short circuit and MPP current (I_{sc}, I_{mp})	5.96, 5.58 A	Hidden neurons (j)	5
Simulation sampling time (T_s)	1 μs	Number of layers (k)	2
Grid voltage (v_g)	20 kV	Output neurons (l)	3
Filter inductance parameters (L_f, R_f)	0.7 mH, 0.003 Ω	μ_{max}, $epoch_{max}$	10^{10}, 1000
Filter capacitance (C_f)	50 μF	λ_1, λ_2	4, 0
DC-link capacitance (C_{dc})	3 mF	Min. gradient value, K_p, K_i	10^{-10}, 2, 15
Converter efficiency (η)	0.95	V_{PV}^{Low}, V_{PV}^{High}, V_{step}	360, 700, 20 V

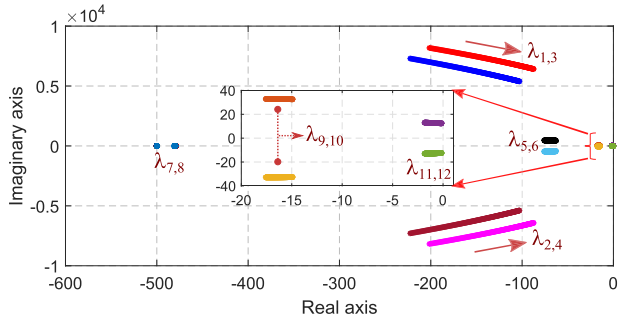

FIGURE 4. Trajectory of eigenvalues under grid-inductance variation.

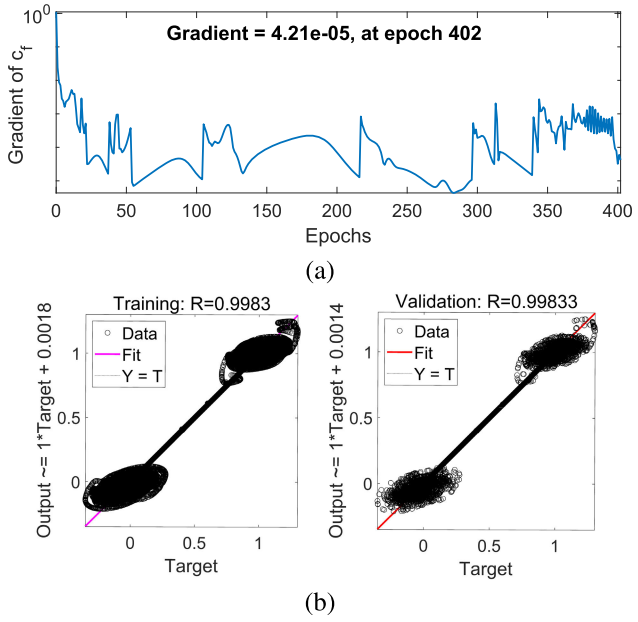

FIGURE 5. Learning profile of the selected ANN structure, (a) Gradient curve, (b) Regression plot.

domain by means of a 12th order non-linear model. But, the non-linearity associated with this model restricts the direct application of traditional linear methods. Thus, the small-signal representation of the model can be written as

$$\Delta \dot{x_{ss}} = \mathbf{A_{ss}}.\Delta x_{ss} + \mathbf{B_{ss}}.\Delta u_{ss} \tag{23}$$

where x_{ss} is the state vector, $\mathbf{A_{ss}}$ is system matrix, u_{ss} is input vector, $\mathbf{B_{ss}}$ is input matrix, and Δ represents the small-signal perturbation around the steady-state value.

A detailed derivation of all the state-space equations for a grid-connected VSC system with only current controller

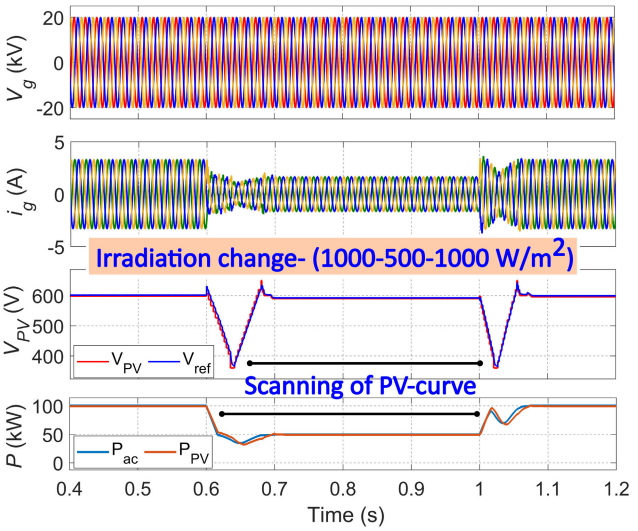

FIGURE 6. Results with proposed controller under sudden irradiation change.

can be found in [8] and [29]. In this work, the state-space equation related to the PI-loop used after the MPPT stage is newly added. Accordingly, the state-space equations are reformulated and presented by

$$\begin{aligned} x_{ss} &= [v_{f\alpha}\ \ v_{f\beta}\ \ i_{o\alpha}\ \ i_{o\beta}\ \ \gamma\ \ i_{f\alpha}\ \ i_{f\beta}\ \ v_{PLL,1}\ \ v_{PLL,2} \\ &\quad \epsilon_{PLL}\ \ \Delta\theta_{PLL}\ \ v_{dc}]^T \\ u_{ss} &= [v_{ref}\ \ v_g\ \ \omega_g]^T \end{aligned} \tag{24}$$

where $v_{PLL,1}$, $v_{PLL,2}$, ϵ_{PLL}, $\Delta\theta_{PLL}$ are the state variables related to the PLL, γ is the integrator state of the dc-side PI-loop, and ω_g is the grid frequency.

The eigenvalues of $\mathbf{A_{ss}}$ can be considered to examine the behaviour of the system and controller. The analytically calculated eigenvalues are listed in Table 1. Participation factors are calculated to assess the relative contribution of different states in each mode. The contributions from the dominant states are also listed for all the modes.

As observed from the relative contribution values, the high and medium frequency modes (λ_{1-6}) are influenced mainly by the point of common coupling (PCC) capacitor voltage, output current and grid current. Modes λ_{7-10} are related to the low pass filters (LPF) and integrator used in the PLL. This, along with the participation factors, points out that the modes λ_{11-12} are affected by the dc-side capacitor voltage and

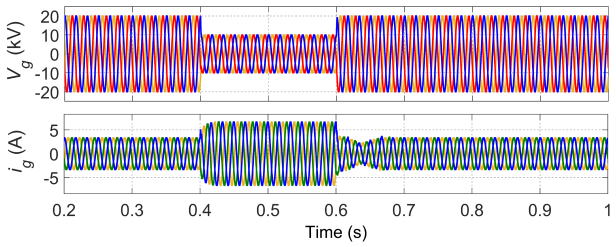

FIGURE 7. Performance of proposed controller under grid-side fault condition.

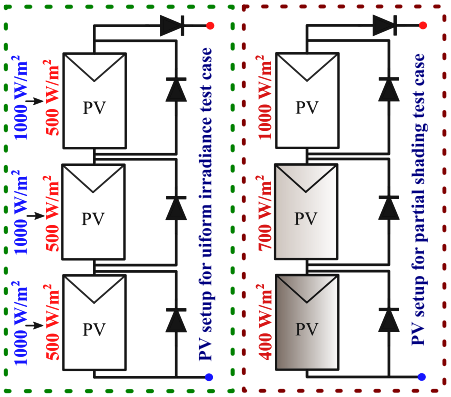

FIGURE 8. PV setup for uniform and partial shading test cases.

PI-loop. Nonetheless, all the eigenvalues are in the negative half of the complex plane, indicating the system is stable. Further, the grid-side inductance (L_o) value is varied from 0.2 to 1 mH in the eigenvalues trajectory shown in Fig. 4. It can be observed that the modes λ_{1-4} are mainly affected and moves towards the origin with the increase in L_o value, but are still in the negative-half. This indicates the system is stable even under extremely weak grid conditions.

VI. SIMULATION RESULTS AND DISCUSSION

The proposed ANN controller for the SSGT PV system as shown in Fig. 1 was implemented in MATLAB/Simulink platform using the SimPower systems Toolbox. The Sun-Power SPR-305E model is used as a PV panel in the configuration of 66 parallel strings and 5 series modules per string forming a 100 kW rated power system. All the parameters of the investigated SSGT PV system are presented in Table 2.

A. DATA COLLECTION AND FINALIZATION OF ANN STRUCTURE

A total of 100000 data points are stored in a look-up table that is obtained by executing the MPC scheme under changing irradiance level, grid voltage sag, swell and fault conditions. The data set is further divided into three parts: a training set (70% of total data), a validation set (15%), and a test set (15%). The training set is used to determine the weight update at each iteration. The validation set is an indicator of what is happening to the network function in-between the training epoch, and its error is monitored during the training

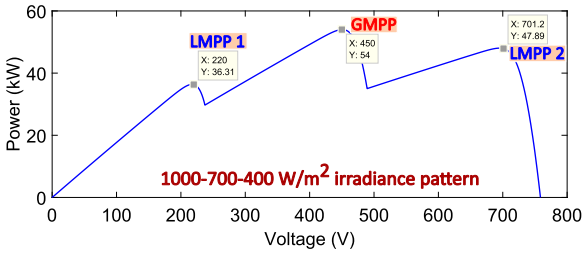

FIGURE 9. Ideal PV-curve under partial shading of the SSGT system.

process. Fig. 5 shows the learning profile of the selected ANN structure. The gradient of the cost function dropped to a lower value within 500 iterations, which can be verified from Fig. 5(a). Further, regression (R) value defines the prediction precision of the ANN and closer to unity defines a closer relationship. Fig. 5(b) illustrates the R is near to unity indicating a successful training of employed ANN.

B. ANALYSIS UNDER DYNAMIC CHANGING CONDITIONS

The performance of the proposed ANN controller is tested under variation of irradiation pattern and grid side voltage change when the PV array is uniformly shaded. Fig. 6 shows the grid voltage (V_g), current injected to the grid (i_g), dc voltage or PV voltage (V_{PV}), PV power (P_{PV}), and output power (P_{ac}) under the step irradiation change condition. The current magnitude changes proportionally without deteriorating its desired shape. The V_g profile is unaffected during this incident and the proposed control strategy quickly scans the new MPP, which is evident from the V_{PV} and P_{PV} profile. On the other hand, the dc-side parameters are maintained at a steady-state value all along with this test interval. Fig. 7 shows satisfactory working under grid-side fault conditions, where voltage magnitude is decreased by 50 % during 0.4 to 0.6 s. During this period, the current injection to the grid is increased proportionally to maintain the constant power flow, indicating the low-voltage ride through ability of the proposed controller. It is worth mentioning that, the recorded total harmonic distortion (THD) level of the injected grid current in steady-state is 3.1 % which complies with IEEE-519 standard.

C. COMPARATIVE ANALYSIS UNDER PARTIAL SHADING CONDITION

The effectiveness of the proposed controller is also tested under partial shading conditions. It is compared with the widely-used PI-controller implemented with optimized parameters in the benchmark model [30], MPC scheme, and the support vector machine-based ML (SVM-ML) controller integrated with the P&O MPPT algorithm. The SVM-ML is implemented by taking the reference of [31]. Moreover, three PV-panels (each having 30 parallel strings and four series modules per string) are cascaded to form the rated SSGT PV system for performing the partial shading test, as illustrated in Fig. 8. Among the three cascaded PV-panels, two are partially shaded, and the same structure is considered

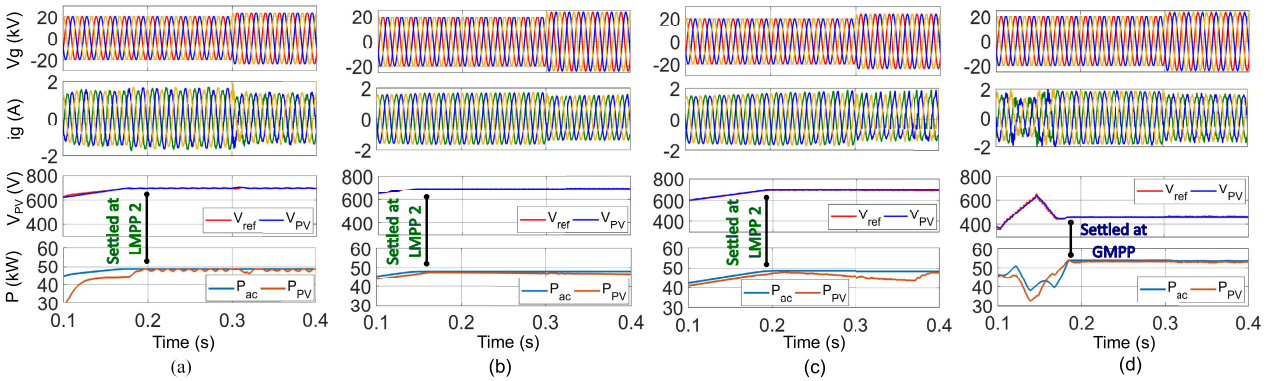

FIGURE 10. Comparative performance analysis under partial shading condition obtained with, (a) PI-controller, (b) MPC controller, (c) SVM-ML controller, (d) Proposed controller.

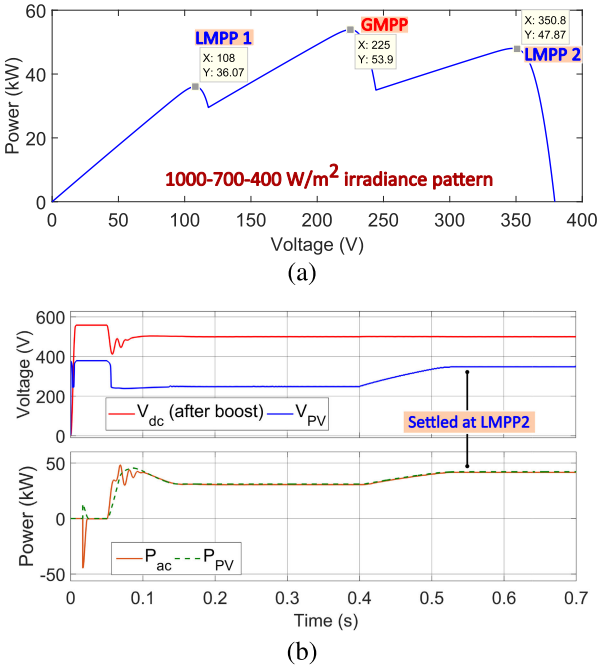

FIGURE 11. Performance of the benchmark model under partial shading, (a) ideal PV-curve, (b) actual PV-profile.

for all the controllers to execute a fair comparative analysis. The ideal PV-curve in Fig. 9 indicates there are two LMPPs, and the power at the GMPP is $\approx$ 54 kW for the considered irradiation pattern. In this context, the PI-based controller, MPC-based control scheme, SVM-ML controller settles at the LMPP2 (350.8 V, 47.87 kW) instead of GMPP, as shown in Fig. 10(a-c). On the other hand, the proposed ANN-based controller accurately tracks the GMPP (450 V, 54 kW) within a short time, which is evident from Fig. 10(d). Further, a grid voltage swell of 0.2 p.u. is created in V_g at 0.3 s. The grid-side voltage, current, and power profile of the proposed ANN controller are found to be satisfactory as compared to the other three controllers.

Additionally, the benchmark model is also tested under the same irradiation pattern. The benchmark model is a double-stage PV system, where the InC MPPT algorithm is implemented to generate the duty cycle for the dc-dc converter [30]. From Fig. 11, the controller reaches the steady-state operating point very late and settles at the LMPP2 (350.8 V, 47.87 kW) instead of GMPP. This further justifies the superior performance of the proposed control system.

D. VALIDATION UNDER REAL WORLD DATA

The proposed controller performance is further validated under a realistic scenario. This test case is performed by considering the solar irradiation and temperature data of 1st June 2021 received on the solar power plant installed on the rooftop of the Norwegian University of Science and Technology (NTNU), Trondheim, Norway. The irradiation and temperature profile on the mentioned date is illustrated in Fig. 12(a). The proposed controller is still able to maintain the grid voltage and current at the desired level without making the system unstable, which is evident from Fig. 12(b). Despite the highly dynamic PV-profile, the MPP is scanned at every changing scenario and the power is maintained in accordance with the irradiance profile.

E. COMPUTATIONAL COMPLEXITY EVALUATION

Expressions in (8), (9), and (18) are used to evaluate the overall computational complexity. For a 2L converter control, MPC needs to evaluate the $2^3 = 8$ switching states. In this aspect, the prediction and cost function is also solved 8 times. Thus, the total number of calculations involved in the MPC control in one sampling period is $\geqslant$ 192 (prediction horizon length is 1). Conversely, as the proposed ANN controller uses 7 inputs (i) and 3 inputs (l), total number of calculations by the ANN controller in terms of hidden neurons (j) is $24j$. In this work, value of $j = 5$ gives the best approximation. Hence, the total number of calculations by the ANN controller is 120. This implies, the proposed ANN controller lessens the calculations as compared to MPC. Additionally, the calculations associated with the MPC are mainly optimization-based and are complex for higher-order systems, whereas simple addition and multiplication types of calculations are involved in the ANN controller.

TABLE 3. Efficiency evaluation of the SSGT PV system with proposed controller.

$\%P_{out}$	5%	10%	20%	30%	50%	100%	$\eta_{EU}(\%)$
-	5kW	10kW	20kW	30kW	50kW	100kW	-
w_e	0.03	0.06	0.13	0.1	0.48	0.2	-
$\eta(\%)$	93.31	95.02	96.83	98.42	97.52	98.21	97.38

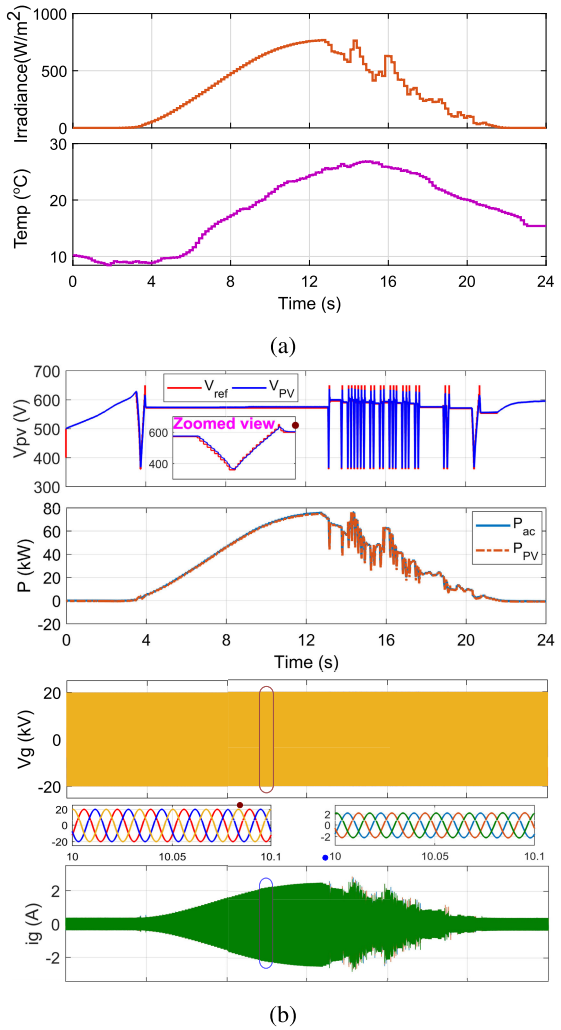

FIGURE 12. Performance of the proposed controller under the real-world solar irradiation and temperature data received on 1st June 2021, on the rooftop of NTNU, Trondheim, (a) Irradiation and temperature profile, (b) Actual time domain results.

F. EFFICIENCY CALCULATION

One of the standard efficiency calculation method for grid-connected PV systems is Weighted European Efficiency (η_{EU}), in which, efficiency at different operating power is noted, and are then multiplied with the corresponding pre-defined weight values (w_e) [32]. The overall efficiency of the SSGT PV system with the proposed control system is summarized in Table 3. It can be seen that the overall efficiency is high in the entire operating range.

VII. EXPERIMENTAL RESULTS WITH C-HIL TEST

Experimental analysis based on a control-hardware in the loop (C-HIL) approach is carried out to validate the effectiveness of the proposed ANN-based controller. The C-HIL setup picture is presented in Fig. 13. The OPAL-RT platform is used to emulate the power stage (PV, VSC, and grid) using the standard RT-LAB and MATLAB library tools. The power stage is discretised with a sampling time of 1 μ s to mimic similar to the real-hardware system. The proposed control system is programmed inside an Arduino controller, where the MPPT stage runs with a sampling time of 1000 μ s and the ANN controller runs at 100 μ s. By receiving the desired analogue signals as input, the Arduino executes the proposed control system to determine the PWM signals

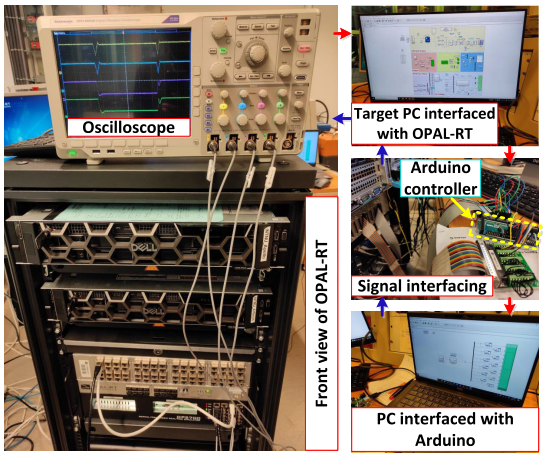

FIGURE 13. C-HIL setup using OPAL-RT platform and Arduino mega-2560 controller.

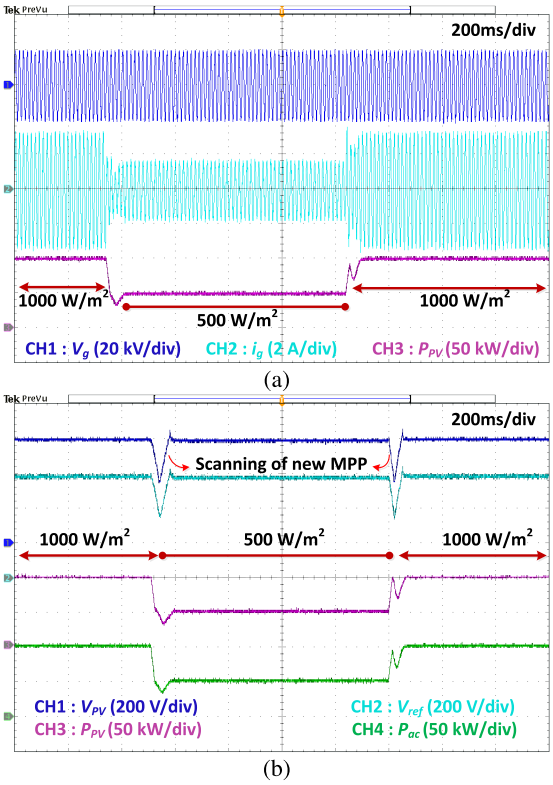

FIGURE 14. Experimental results under step irradiation change, (a) V_g,i_g and P_{PV}, (b) V_{PV},V_{ref}, P_{PV} and P_{ac}.

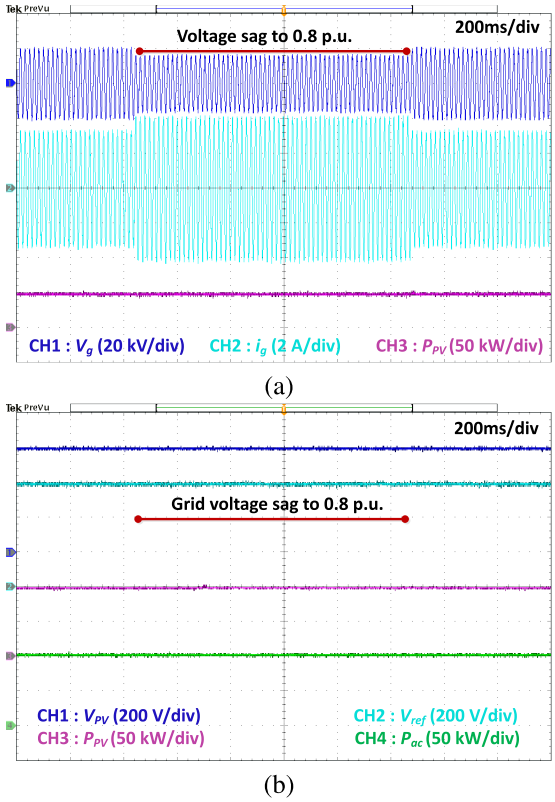

FIGURE 15. Experimental results under grid voltage sag, (a) V_g,i_g and P_{PV}, (b) V_{PV},V_{ref}, P_{PV} and P_{ac}.

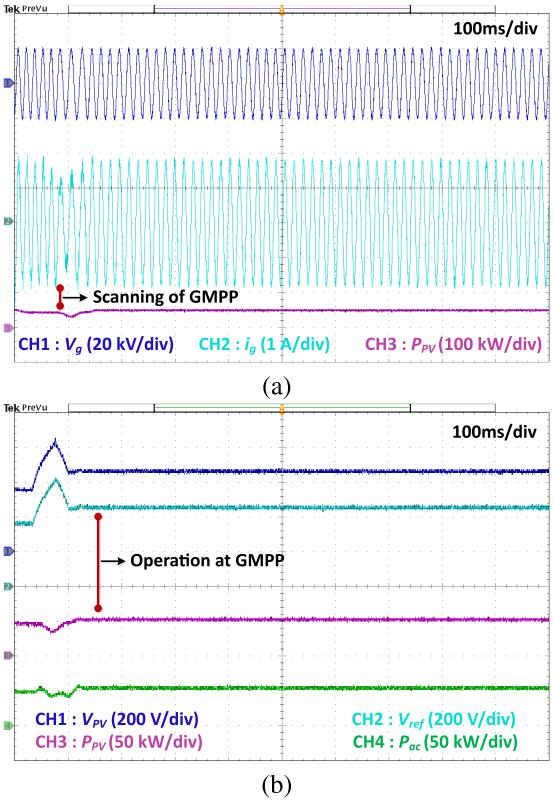

FIGURE 17. Experimental results under partial shading condition, (a) V_g,i_g and P_{PV}, (b) V_{PV},V_{ref}, P_{PV} and P_{ac}.

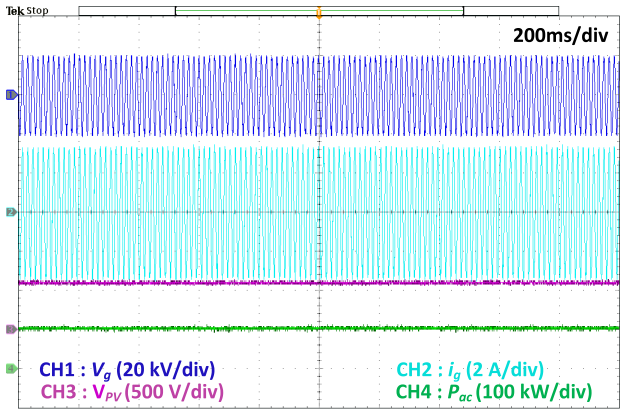

FIGURE 16. Experimental results under parameter uncertainty.

for the converter, which is emulated inside the OPAL-RT platform. In this fashion, the control loop is closed and prototypical results are obtained for different test scenarios.

Fig. 14 shows the real-time performance of the proposed ANN controller under a step change in irradiation. The grid voltage is stable and is not much influenced by this change, although the current magnitude and power level change in accordance with the irradiation level. The satisfactory performance of the ANN controller under grid voltage fluctuation can be verified from Fig. 15. As shown in Fig. 15(a), the grid voltage is subjected to a temporary voltage sag to 0.8 p.u. It can be noticed that the magnitude of grid current is elevated during this interval to maintain the power level. Nonetheless, the PV voltage and power are unaffected as can be seen from Fig. 15(b). Moreover, the filter parameters are changed to 30% of their rated value as mentioned in the Table 2 and the obtained results are depicted in Fig. 16. The robust performance of the proposed controller can be observed from this test case as all the signals are maintained within the desired level.

Furthermore, to assess the efficacy of the proposed controller under partial shading conditions, two of the PV modules are partially shaded as done in the simulation study, and the obtained results are demonstrated in Fig. 17. In such a case, the proposed controller is still able to extract the optimum power ($\approx$ 54 kW) from the PV-array and smoothly transfers it to the grid by maintaining the stable grid-side voltage and current signals. Besides, the proposed controller starts scanning the GMPP at the beginning as illustrated in Fig. 17(b) and reaches the steady-state GMPP within a short time interval.

VIII. CONCLUSION

In this work, a novel ANN-based controller integrated with an improved MPPT controller has been presented for an SSGT PV system. The ANN structure is trained offline using data from a supervisory MPC scheme. The ANN controller is deployed in real-time upon successful training, eliminating the need for a complex and computationally intensive MPC

scheme. The proposed ANN controller reduces the number of calculations by 1.6 times that of the traditional MPC, offering a more efficient solution. Comparative simulation studies show that the ANN controller achieves fast and accurate tracking performance, outperforming standard controllers. Furthermore, the ANN controller demonstrates robust performance under realistic irradiation and temperature patterns, confirming its suitability for practical applications. Comprehensive C-HIL experiments, which consider various PV-side and grid-side dynamics, validate the real-time effectiveness of the proposed ANN controller. These results highlight the ANN controller's potential for improving the efficiency and reliability of SSGT PV systems in real-world conditions.

REFERENCES

[1] H. Pan, X. Feng, F. Li, and J. Yang, "Energy coordinated control of DC microgrid integrated incorporating PV, energy storage and EV charging," *Appl. Energy*, vol. 342, Jul. 2023, Art. no. 121155, doi: 10.1016/j.apenergy.2023.121155.

[2] S. K. Sahoo, S. Sukchai, and F. F. Yanine, "Review and comparative study of single-stage inverters for a PV system," *Renew. Sustain. Energy Rev.*, vol. 91, pp. 962–986, Aug. 2018, doi: 10.1016/j.rser.2018.04.063.

[3] R. Bradai, R. Boukenoui, A. Kheldoun, H. Salhi, M. Ghanes, J.-P. Barbot, and A. Mellit, "Experimental assessment of new fast MPPT algorithm for PV systems under non-uniform irradiance conditions," *Appl. Energy*, vol. 199, pp. 416–429, Aug. 2017, doi: 10.1016/j.apenergy.2017.05.045.

[4] H. Ghoddami and A. Yazdani, "A single-stage three-phase photovoltaic system with enhanced maximum power point tracking capability and increased power rating," *IEEE Trans. Power Del.*, vol. 26, no. 2, pp. 1017–1029, Apr. 2011, doi: 10.1109/TPWRD.2010.2055896.

[5] B. P. Singh, S. K. Goyal, S. A. Siddiqui, A. Saraswat, and R. Ucheniya, "Intersection point determination method: A novel MPPT approach for sudden and fast changing environmental conditions," *Renew. Energy*, vol. 200, pp. 614–632, Nov. 2022, doi: 10.1016/j.renene.2022.09.056.

[6] Q. Li, S. Zhao, M. Wang, Z. Zou, B. Wang, and Q. Chen, "An improved perturbation and observation maximum power point tracking algorithm based on a PV module four-parameter model for higher efficiency," *Appl. Energy*, vol. 195, pp. 523–537, Jun. 2017, doi: 10.1016/j.apenergy.2017.03.062.

[7] A. Refaat, Q. A. Ali, M. M. Elsakka, Y. Elhenawy, T. Majozi, N. V. Korovkin, and M. H. Elfar, "Extraction of maximum power from PV system based on horse herd optimization MPPT technique under various weather conditions," *Renew. Energy*, vol. 220, Jan. 2024, Art. no. 119718, doi: 10.1016/j.renene.2023.119718.

[8] P. R. Bana and M. Amin, "Control for grid-connected VSC with improved damping based on physics-informed neural network," *IEEE J. Emerg. Sel. Topics Ind. Electron.*, vol. 1, no. 2, pp. 1–11, Jul. 2023, doi: 10.1109/JESTIE.2023.3258339.

[9] M. F. Umar, M. Easley, B. Nun, A. Khan, M. B. Shadmand, S. Bayhan, and H. Abu-Rub, "Single-phase grid-interactive inverter with resonance suppression based on adaptive predictive control in weak grid condition," *IEEE J. Emerg. Sel. Topics Ind. Electron.*, vol. 3, no. 3, pp. 809–820, Jul. 2022, doi: 10.1109/JESTIE.2021.3103675.

[10] A. M. Diab, S. S. Yeoh, S. Bozhko, C. Gerada, and M. Galea, "Enhanced active disturbance rejection current controller for permanent magnet synchronous machines operated at low sampling time ratio," *IEEE J. Emerg. Sel. Topics Ind. Electron.*, vol. 3, no. 2, pp. 230–241, Apr. 2022, doi: 10.1109/JESTIE.2021.3063919.

[11] S. Vazquez, J. Rodriguez, M. Rivera, L. G. Franquelo, and M. Norambuena, "Model predictive control for power converters and drives: Advances and trends," *IEEE Trans. Ind. Electron.*, vol. 64, no. 2, pp. 935–947, Feb. 2017, doi: 10.1109/TIE.2016.2625238.

[12] S. Bayhan and H. Abu-Rub, "Predictive control of power electronic converters," in *Power Electronics Handbook*, 4th ed. London, U.K.: Butterworth, 2018, pp. 1325–1338.

[13] D. Wang, Z. J. Shen, X. Yin, S. Tang, X. Liu, C. Zhang, J. Wang, J. Rodriguez, and M. Norambuena, "Model predictive control using artificial neural network for power converters," *IEEE Trans. Ind. Electron.*, vol. 69, no. 4, pp. 3689–3699, Apr. 2022, doi: 10.1109/TIE.2021.3076721.

[14] A. Laib, A. Krama, A. Sahli, A. Kihal, and H. Abu-Rub, "Reconfigurable model predictive control for grid connected PV systems using thirteen-level packed E-Cell inverter," *IEEE Access*, vol. 10, pp. 102210–102222, 2022, doi: 10.1109/ACCESS.2022.3208106.

[15] H. Bai, C. Liu, E. Breaz, and F. Gao, "Artificial neural network aided real-time simulation of electric traction system," *Energy AI*, vol. 1, Aug. 2020, Art. no. 100010, doi: 10.1016/j.egyai.2020.100010.

[16] S. Zhao, F. Blaabjerg, and H. Wang, "An overview of artificial intelligence applications for power electronics," *IEEE Trans. Power Electron.*, vol. 36, no. 4, pp. 4633–4658, Apr. 2021, doi: 10.1109/TPEL.2020.3024914.

[17] E. Mohammadi, M. Alizadeh, M. Asgarimoghaddam, X. Wang, and M. G. Simoes, "A review on application of artificial intelligence techniques in microgrids," *IEEE J. Emerg. Sel. Topics Ind. Electron.*, vol. 3, no. 4, pp. 878–890, Oct. 2022, doi: 10.1109/JESTIE.2022.3198504.

[18] M. R. G. Meireles, P. E. M. Almeida, and M. G. Simoes, "A comprehensive review for industrial applicability of artificial neural networks," *IEEE Trans. Ind. Electron.*, vol. 50, no. 3, pp. 585–601, Jun. 2003, doi: 10.1109/tie.2003.812470.

[19] D. Wang, X. Yin, S. Tang, C. Zhang, Z. J. Shen, J. Wang, and Z. Shuai, "A deep neural network based predictive control strategy for high frequency multilevel converters," in *Proc. IEEE Energy Convers. Congr. Expo. (ECCE)*, Sep. 2018, pp. 2988–2992, doi: 10.1109/ECCE.2018.8558293.

[20] J. Chen, Y. Chen, L. Tong, L. Peng, and Y. Kang, "A backpropagation neural network-based explicit model predictive control for DC–DC converters with high switching frequency," *IEEE J. Emerg. Sel. Topics Power Electron.*, vol. 8, no. 3, pp. 2124–2142, Sep. 2020.

[21] M. N. Ali, "Improved design of artificial neural network for MPPT of grid-connected PV systems," in *Proc. 20th Int. Middle East Power Syst. Conf. (MEPCON)*, Dec. 2018, pp. 97–102, doi: 10.1109/MEPCON.2018.8635202.

[22] S. A. Rizzo and G. Scelba, "ANN based MPPT method for rapidly variable shading conditions," *Appl. Energy*, vol. 145, pp. 124–132, May 2015, doi: 10.1016/j.apenergy.2015.01.077.

[23] S. Allahabadi, H. Iman-Eini, and S. Farhangi, "Fast artificial neural network based method for estimation of the global maximum power point in photovoltaic systems," *IEEE Trans. Ind. Electron.*, vol. 69, no. 6, pp. 5879–5888, Jun. 2022, doi: 10.1109/TIE.2021.3094463.

[24] M. Ali, M. Tariq, K. A. Lodi, R. K. Chakrabortty, M. J. Ryan, B. Alamri, and C. Bharatiraja, "Robust ANN-based control of modified PUC-5 inverter for solar PV applications," *IEEE Trans. Ind. Appl.*, vol. 57, no. 4, pp. 3863–3876, Jul. 2021, doi: 10.1109/TIA.2021.3076032.

[25] Y. Sun, S. Li, B. Lin, X. Fu, M. Ramezani, and I. Jaithwa, "Artificial neural network for control and grid integration of residential solar photovoltaic systems," *IEEE Trans. Sustain. Energy*, vol. 8, no. 4, pp. 1484–1495, Oct. 2017, doi: 10.1109/TSTE.2017.2691669.

[26] M. Nauman and A. Hasan, "Efficient implicit model-predictive control of a three-phase inverter with an output LC filter," *IEEE Trans. Power Electron.*, vol. 31, no. 9, pp. 6075–6078, Sep. 2016, doi: 10.1109/TPEL.2016.2535263.

[27] C. Xue, L. Ding, and Y. Li, "CCS-MPC with long predictive horizon for grid-connected current source converter," in *Proc. IEEE Energy Conv. Congr. Expo.*, Jul. 2020, pp. 4988–4993, doi: 10.1109/ECCE44975.2020.9235774.

[28] S. Vanti, P. R. Bana, S. D'Arco, and M. Amin, "Single-stage grid-connected PV system with finite control set model predictive control and an improved maximum power point tracking," *IEEE Trans. Sustain. Energy*, vol. 13, no. 2, pp. 791–802, Apr. 2022, doi: 10.1109/TSTE.2021.3132057.

[29] P. Ranjan Bana, M. Amin, and M. Molinas, "ANN-based surrogate PI and MPC controllers for grid-connected VSC system: Small-signal analysis and comparative evaluation," *IEEE J. Emerg. Sel. Topics Power Electron.*, vol. 12, no. 1, pp. 566–578, Feb. 2024, doi: 10.1109/jestpe.2023.3328260.

[30] P. Giroux, G. Sybille, C. Osorio, and S. Chandrachood, *Detailed Model of a 100-Kw Grid-Connected PV Array*. Natick, MA, USA: MathWorks. Accessed: Feb. 2021.

[31] T. Mathworks. (2015). *Fit a Support Vector Machine Regression Model*. [Online]. Available: https://se.mathworks.com/help/stats/fitrsvm.html

[32] M. N. H. Khan, M. Forouzesh, Y. P. Siwakoti, L. Li, T. Kerekes, and F. Blaabjerg, "Transformerless inverter topologies for single-phase photovoltaic systems: A comparative review," *IEEE J. Emerg. Sel. Topics Power Electron.*, vol. 8, no. 1, pp. 805–835, Mar. 2020, doi: 10.1109/JESTPE.2019.2908672.

PRABHAT RANJAN BANA received the bachelor's degree in electrical engineering from the Parala Maharaja Engineering College, Berhampur, India, in 2016, the master's degree in power and energy systems from the National Institute of Technology (NIT) Meghalaya, India, in 2019, and the Ph.D. degree from the Department of Electric Energy, Norwegian University of Science and Technology, Norway, in 2024.

From January 2019 to March 2019, he was a Visiting Scholar with Cardiff University, Cardiff, U.K., funded through the Joint U.K.–India Clean Energy (JUICE) two-month exchange program scheme. From July 2019 to February 2020, he was a Research Fellow with NIT Meghalaya. Since November 2023, he has been a Research and Development Engineer with Hitachi Energy, Västerås, Sweden. His research interests include multilevel inverters, photovoltaic systems, and advanced control of power electronics systems.

SALVATORE D'ARCO received the M.Sc. and Ph.D. degrees in electrical engineering from the University of Naples Federico II, Naples, Italy, in 2002 and 2005, respectively.

From 2006 to 2007, he was a Postdoctoral Researcher with the University of South Carolina, Columbia, SC, USA. In 2008, he joined ASML, Veldhoven, The Netherlands, as a Power Electronics Designer Consultant, where he worked, until 2010. From 2010 to 2012, he was a Postdoctoral Researcher with the Department of Electric Power Engineering, Norwegian University of Science and Technology (NTNU), Trondheim, Norway. In 2012, he joined SINTEF Energy Research, Trondheim, where he is currently a Senior Research Scientist. He is the author of more than 130 scientific papers and is the holder of one patent. His main research interests include control and analysis of power-electronic conversion systems for power system applications, including real-time simulation and rapid prototyping of converter control systems.

MOHAMMAD AMIN (Senior Member, IEEE) received the B.Sc. degree in electrical and electronic engineering from Chittagong University of Engineering and Technology, Chittagong, Bangladesh, in 2008, the M.Sc. degree in electric power engineering from the Chalmers University of Technology, Gothenburg, Sweden, in 2011, and the Ph.D. degree in engineering cybernetics from the Norwegian University of Science and Technology, Trondheim, Norway, in 2017.

From 2008 to 2013, he was with the Department of Electrical and Electronic Engineering International Islamic University Chittagong, Chittagong, Bangladesh. In 2015, he was a Ph.D. Visiting Scholar with the Wind Power Research Center, Shanghai Jiao Tong University, Shanghai, China. From 2017 to 2019, he was a Senior Research Associate with the Department of Electrical and Computer Engineering, Illinois Institute of Technology, Chicago, IL, USA. He was an Associate Professor with the Department of Electric Power Engineering, Norwegian University of Science and Technology, from 2019 to 2022. He was also a Visiting Associate with the University of Minnesota, in Summer 2022. He is currently with Enchanted Rock Management LLC, Houston, TX, USA. His research interests include power electronics application to power systems, application of artificial intelligence in power electronics systems, microgrids, smart grids, robust integration of battery energy storage systems, wind and solar energy, and robust control theory for power electronics systems.

Dr. Amin was a recipient of the 2018 IEEE JESTPE First Prize Paper Award from the IEEE Power Electronics Society and the 2020 Premium Award for Best Paper in *IET Generation, Transmission and Distribution*.